Journal of Colloid and Interface Science **238,** 251–258 (2001)
doi:10.1006/jcis.2001.7482, available online at http://www.idealibrary.com on IDEAL®

Structural Changes Induced in the Surfactant System $C_{12}E_4$/Benzyl Alcohol/Water by the Admixture of the Cationic Surfactant Cetylpyridinium Chloride

G. Montalvo,*,[1] M. Valiente,* K. Mortensen,† and M. Gradzielski‡

*Departamento de Química Física, Universidad de Alcalá, E-28871 Madrid, Spain; †Condensed Matter Physics and Chemistry Department, Risø National Laboratory, DK-4000 Roskilde, Denmark; and ‡Lehrstuhl für Physikalische Chemie I, Universität Bayreuth, D-95440 Bayreuth, Germany

Received June 27, 2000; accepted February 14, 2001

The influence of the addition of the cationic surfactant cetylpyridinium chloride (CPyCl) on the structure of the different phases of the ternary surfactant system $C_{12}E_4$/benzyl alcohol/water in the dilute region has been studied by means of small angle neutron scattering (SANS) and freeze-fracture microscopy (FF-TEM). In the ternary system various different subregions of the L_α-phase were identified as a function of the concentration of the cosurfactant, benzyl alcohol. Addition of small amounts of CPyCl suppresses these different L_α-phases in favor of the one composed of multilamellar vesicles. Addition of somewhat larger amounts (up to 2 mol% relative to the total surfactant concentration) destabilizes the formation of bilayer structures completely and leads to the formation of micellar solutions. This demonstrates that in this surfactant system the incorporation of very small amounts of cationic surfactant has a pronounced and systematic fluence on its phase behavior and its structures.

Key Words: **tetraethylene glycol monododecyl ether ($C_{12}E_4$), cetylpyridinium chloride (CPyCl), lamellar phase, vesicles, open bilayers, SANS, FF-TEM, thickness of membranes.**

I. INTRODUCTION

In many cases micelles are formed when amphiphilic surfactant molecules are dissolved in water (1). These self-assembled aggregates can be of different shapes such as spherical, wormlike, or disklike. Another possible form of aggregation is the formation of bilayer structures. For instance, for a binary nonionic polyoxyethylene surfactant, under dilute conditions, the formation of liquid crystalline lamellar phases, of vesicle phases or of sponge phases (L_3-phase), has been observed which all are composed of surfactant bilayers (2). The sponge L_3-phase is flow birefringent and made up from a random bicontinuous microstructure of surfactant bilayers (3). The classical lamellar L_α-phase is anisotropic and consists of stacked surfactant bilayers.

Medium chain alcohols acting as cosurfactants had been used previously in ternary systems as $C_{12}E_4$/alcohol/water (4, 5). In their presence, the lamellar phase can be subdivided into various different subregions, and by increasing the amount of alcohol exhibits the sequence L_α^+–$L_{\alpha l}$–$L_{\alpha h}$ (6). Its microstructure changes from unilamellar vesicles (L_α^+) (7) to multilamellar vesicles ($L_{\alpha l}$) (8) and to stacked bilayers ($L_{\alpha h}$). Macroscopically the birefringence increases along this phase progression more or less continuously and sometimes the boundaries are difficult to determine by visual inspection.

Recently we studied the effect of benzyl alcohol on the formation of these kinds of bilayer-type structures with dodecyl tetraethylene glycol ($C_{12}E_4$) as surfactant (9). Benzyl alcohol has been shown before to be an interesting cosurfactant, as, for instance, it allows a direct transition from normal to reverse micelles without phase separation in CTAB (10). From these results we concluded that the benzyl alcohol stabilizes bilayer structures over a larger concentration range than corresponding medium-chain alcohols with straight alkyl chains. Rheological experiments were performed in the various subregions of the L_α-phase and were shown to be a good tool to determine the borders of the different lamellar subregions. In addition, shear-induced structural changes were observed (9).

In a next step we introduced ionic charges into the system by admixing the cationic surfactant cetylpyridinium chloride (CPyCl). The phase diagram of the $C_{12}E_4$/CPyCl/benzyl alcohol/water system, at $[C_{12}E_4] = 50$ mM and $25.0 \pm 0.1^\circ$C, was reported (11). The presence of CPyCl surfactant stabilizes the closed bilayer structures (vesicles) and thereby leads to disappearance of the $L_{\alpha h}$- and L_3-phase regions. The driving force for these topological transitions is the fact that addition of the cationic surfactant CPyCl increases the charge density of the amphiphilic bilayer. Increasing charge density will influence the bending moduli of the bilayer and in particular lead to a decrease of the Gaussian modulus $\bar{\kappa}$ (12). However, such a decrease of $\bar{\kappa}$ destabilizes $L_{\alpha h}$- and L_3-phases and favors formation of vesicles (13).

At higher CPyCl content an extended normal micellar phase is formed. In this paper we have used primarily the SANS technique and some complementary freeze-fracture electron microscopy to determine the microstructure of the different phases in the ternary and quaternary system.

[1] To whom correspondence should be addressed.

0021-9797/01 $35.00

II. MATERIALS AND METHODS

The nonionic surfactant tetraethylene glycol monododecyl ether ($C_{12}E_4$) was purchased from Nikkol Ltd. The cetylpyridinium chloride (CPyCl) and the benzyl alcohol (p.a.) were from Merck. All the compounds were used without further purification except the cationic surfactant, which was recrystallized from methanol/ether mixtures several times.

Samples were prepared by weighing the desired amounts of nonionic and cationic surfactants and benzyl alcohol in glass graduated tubes and pure distilled water was added to obtain samples of 10 ml. The sample tubes were kept in a $25.0 \pm 0.1^\circ$C water bath until the equilibrium phase were obtained and the phase behavior was determined by visual inspection through crossed polarizers and by optical microscopy with a Laborlux S LEITZ with polarizers.

For the FF-TEM, water was replaced by a water/glycerol solution (15% w/w), i.e., the maximum amount of glycerol that does not affect the phase behavior significantly. Small amounts of sample were placed on a 0.1-mm-thick copper disk covered with a second copper disk. The sample was frozen by plunging this sandwich into liquid propane (cooled by liquid nitrogen). Fracturing and replication were carried out in a Balzers BAF 400 at a temperature of -140°C. Pt/C was deposited at an angle of 45° and 90°, respectively. The formed replicas were examined in a CEM 902 electron microscope (Zeiss).

For the SANS experiments, samples were prepared with D_2O. In the quaternary $C_{12}E_4$ (fixed at 50 mM)/CPyCl/Benzyl alcohol/D_2O system a new batch of nonionic surfactant was used. Both of these factors modified the phase diagram to a considerable extent, as will be described, but the phase sequence remains the same.

SANS experiments in the ternary system were performed at the Laboratoire Léon Brillouin, Saclay, on the PAXY spectrometer. A wavelength of 6 Å was chosen, and sample-to-detector distances of 1.04 and 4.05 m were employed. Thereby we covered a q-range of 0.014–0.35 Å^{-1}.

The SANS experiments in the quaternary system were performed on the SANS instrument of the Risø National Laboratory. In order to cover a large range of momentum transfer, the following combinations of wavelength and sample-to-detector distance were employed: 2.8 Å/1.2 m, 4.7 Å/3.0 m, 4.7 Å/6.0 m, and 17.1 Å/6.0 m. With these configurations we were able to cover a q-range of 0.003–0.35 Å^{-1}.

In both cases the data were recorded on a 128×128 two-dimensional detector. The intensity data were corrected by comparison with the flat scattering of a water standard. Using a proper correction for the detector background and subtracting the scattering of the empty cell they were converted into absolute intensities. However, it should be noted that this intensity is mainly due to the coherent scattering of the samples but also still includes the incoherent background due to the sample itself.

III. RESULTS AND DISCUSSION

III.1. Phase Diagram of the $C_{12}E_4$/CPyCl/Benzyl Alcohol/D_2O (Water) System

The phase diagram of the system $C_{12}E_4$ (fixed at 50 mM)/CPyCl/benzyl alcohol/D_2O at $25.0 \pm 0.1^\circ$C (Fig. 1) was determined by visual observation through crossed polarizers.

In the absence of CPyCl (i.e., along the vertical axis) a very rich phase behavior is exhibited. One observes the following sequence of lamellar subregions with increasing alcohol concentration: L_α^+–$L_{\alpha l}$–$L_{\alpha h}$. The lamellar phase is optically anisotropic and its birefringence increases with the alcohol concentration, but it is difficult to determine the phase boundary between the different subregions precisely just by visual observation. This boundary can more reliably be determined by rheological measurements (9). The L_α^+-phase at low alcohol content is isotropic and it only shows streaming birefringence. The $L_{\alpha l}$-phase is

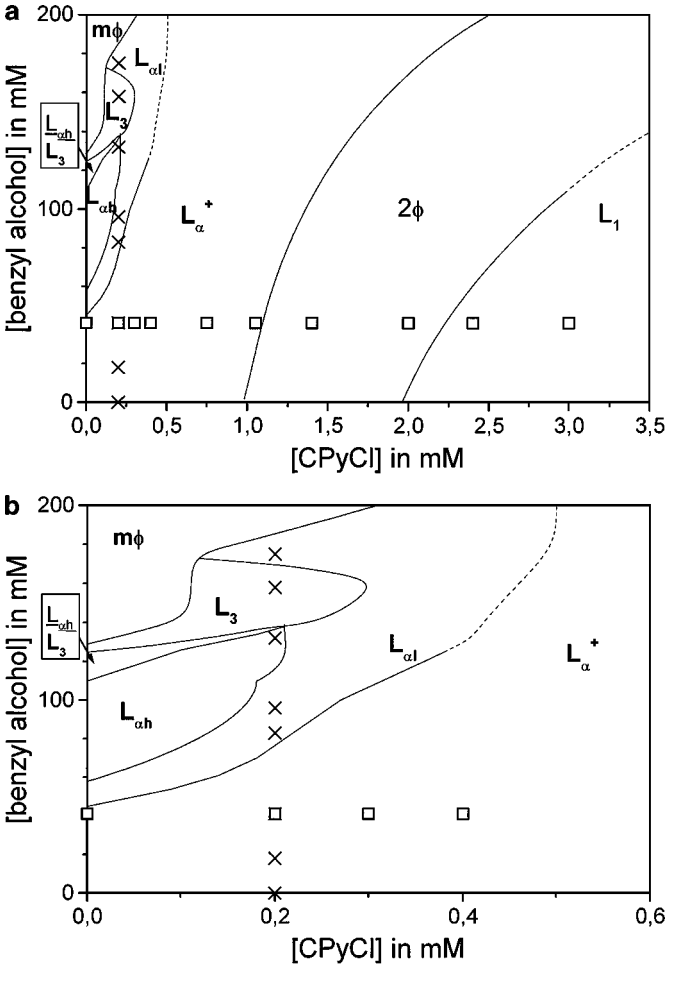

FIG. 1. (a) Phase diagram of the $C_{12}E_4$/CPyCl/benzyl alcohol/D_2O system at $25.0 \pm 0.1^\circ$C for constant concentration of $C_{12}E_4$ ($[C_{12}E_4] = 50$ mM). The points of the SANS investigation are included for the series with [CPyCl] = 0.2 mM (×) and the series with [benzyl alcohol] = 41 mM (□). (b) Extended phase diagram for low content of added CPyCl.

turbid and weakly birefringent. The $L_{\alpha h}$-phase at higher alcohol content is transparent and exhibits strong birefringence in small multidomains. For higher alcohol concentrations a biphasic region $L_{\alpha h}/L_3$ is formed and for still higher alcohol content the isotropic sponge phase (L_3) is formed, which shows flow birefringence. Further addition of benzyl alcohol leads to the formation of multiphase regions (denoted as mϕ in Fig. 1) that do not phase-separate easily and were not further studied in this investigation.

The incorporation of the cationic surfactant disfavors the formation of lamellar phases and of the sponge phase relative to the ternary system. At low concentrations of cationic surfactant, the system still shows the sponge phase and the different lamellar subregions. The $L_{\alpha h}$- and L_3-phases are very flexible and sensitive to shear effects (9). In addition they are very sensitive to the ionic charges (5, 11) and both of them disappear for concentrations of CPyCl larger than 0.2 mM. The electrostatic conditions for the bilayers evidently favor the formation of disconnected structures such as vesicles (14). Similar observations have been made for other surfactant systems upon the addition of ionic surfactant to an originally nonionic surfactant system (5, 15–17). A region of mixed micelles is formed for concentrations of the cationic surfactant higher than 1–1.5 mM. Such an L_1-phase is not observed for the ternary system.

The presence of the D_2O modifies the quaternary phase diagram in some details. As one of the most significant changes, the $L_\alpha^+/2\phi$ and $2\phi/L_1$ phase boundaries move to higher cationic surfactant contents when water (11) is replaced by D_2O (Fig. 1). Moreover, both phase boundaries are almost parallel. The L_α^+-phase solubilizes progressively larger amounts of CPyCl upon increasing the alcohol concentration in the sample, whereas in the system with water, at [alcohol] >25 mM, the L_α^+-phase solubilizes a constant content of CPyCl, 0.4 mM (11). With respect to the $2\phi/L_1$-phase boundary, the dent around 40 mM of alcohol present in the H_2O system (11) disappears in the presence of D_2O (Fig. 1). The shape of the sponge phase is affected as well. It extends to a higher benzyl alcohol content. But these changes are not of profound importance and the principal phase behavior remains identical.

III.2. Structural Investigation of the Ternary System $C_{12}E_4$/Benzyl Alcohol/Water

III.2.1. Freeze-fracture transmission electron microscopy (FF-TEM). The FF-TEM technique was used to obtain information about the microstructure of a sample of the composition 50 mM of $C_{12}E_4$ and 14 mM of benzyl alcohol, i.e., a sample located within the L_α^+-phase. A micrograph is given in Fig. 2. The dominant structure consists of polydisperse and small spherical particles with diameters in the range of 70 to 800 nm. The average is about 100 nm and they are not densely packed. The smaller vesicles have to be unilamellar; some multilamellar structures can be seen for the big ones. Many vesicles are deformed to tubular aggregates, which demonstrates the flexibility of amphiphilic films containing benzyl alcohol. The alcohol molecules are smaller than the surfactant molecules and it appears that they give rise to an increase of the flexibility of the membrane (3). Such an effect of increasing flexibility of amphiphilic films induced by cyclic alcohols such as benzyl alcohol has been deduced from experiments on similar microemulsion systems (18).

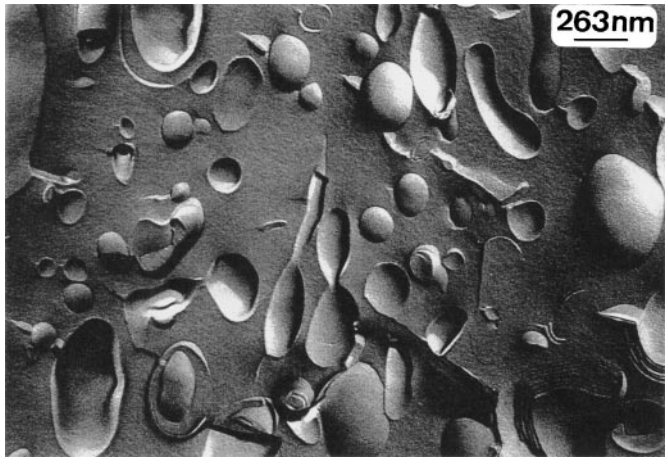

FIG. 2. Electron microscopy micrograph of the sample [$C_{12}E_4$]/[benyzl alcohol] = 50/14 mM, i.e., in the L_α^+ subregion.

In the ternary system, samples at a fixed amount of 150 mM nonionic surfactant have also been studied. The electron microscopy gave evidence that the L_α^+ samples contain mostly unilamellar vesicles, whereas the $L_{\alpha l}$-phase is mainly composed of multilamellar vesicles with diameters between 330 nm and 1000 nm. The samples within the $L_{\alpha h}$-phase contain flat bilayers (19).

III.2.2. Small-angle neutron scattering (SANS). SANS experiments have been carried out in order to obtain more structural information for the different phases in the ternary system, i.e., in the absence of the cationic surfactant. Scattering patterns are isotropic, such as the ones described by Olsson and Mortensen, (20); the azimuthally averaged data are given in Fig. 3a.

In all cases scattering curves are observed where the scattering intensity decreases continuously with increasing q and where the scattering intensity is the lower the higher the content of benzyl alcohol. However, this change in intensity is not continuous and we find two distinct sorts of scattering curves where this change to lower scattering intensities coincides exactly with the macroscopically observed phase transition from $L_{\alpha l}$- to $L_{\alpha h}$-phase which was observed around 60 mM benzyl alcohol. It is interesting to note that the phase of planar bilayers has a scattering intensity that is significantly lower than that of the vesicle phase and thereby the two different phases can clearly be distinguished by means of the scattering experiment.

From the scattering curves (Fig. 3a), the thickness of the bilayers and the effective head group areas of the surfactant molecules have been deduced. To fit the experimental data we employed two different models. Curves were fitted using both a Gaussian (with thickness parameter t, with $D = \sqrt{2\pi} \cdot t$ (21)) and a

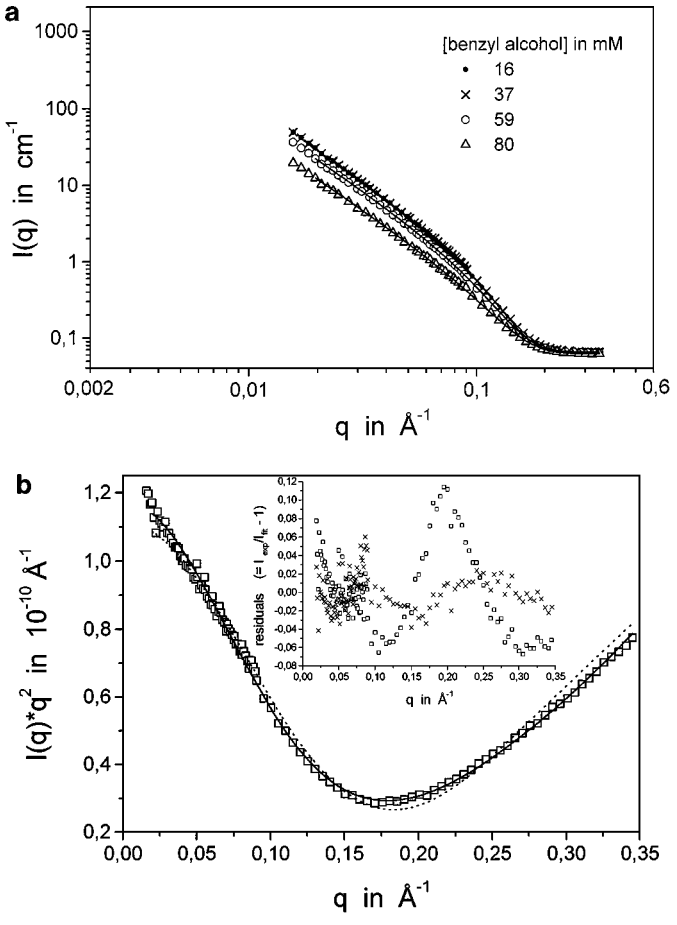

FIG. 3. (a) SANS intensitiy curves for $[C_{12}E_4] = 50$ mM and various amounts of added benzyl alcohol (given in the inset). The samples belong to the following phases: 16 and 37 mM benzyl alcohol, L_α^+ phase; 59 mM benzyl alcohol, $L_{\alpha l}$ phase; and 80 mM benzyl alcohol, $L_{\alpha h}$ phase. (Fit curves according to the Gaussian distribution of the scattering length density are given as solid lines.) (b) Comparison of the fit quality of the models of a Gaussian (solid line) and a rectangular (dotted line) distribution of the scattering length density for the case of the sample of 50 mM $C_{12}E_4$/37 mM benzyl alcohol. For a better representation of the data I^*q^2 is plotted against q. As inset the corresponding residuals (defined by $I_{\text{exp}}/I_{\text{fit}} - 1$) as a function of q are given (×: Gaussian; □: rectangular).

rectangular scattering length profile across the amphiphilic bilayer of a constant thickness D. According to these two models, the scattering intensities are given by

$$I_t(q) = A\frac{2\pi}{q^2}(\Delta\rho)^2 D^2 \exp(-q^2t^2) \qquad [1]$$

$$I_t(q) = A\frac{2\pi}{q^2}(\Delta\rho)^2 D^2 \left(\frac{\sin(qD/2)}{(qD/2)}\right)^2, \qquad [2]$$

where q is the magnitude of the scattering vector, $q = \frac{4\pi n}{\lambda}\sin(\frac{\theta}{2})$; $\Delta\rho$ is the contrast difference between solvent and lamella; and A is the total bilayer area per unit volume, i.e., $A = \frac{2\phi_l}{D}$ (ϕ_l is the total amphiphilic volume fraction). It should be noted that both models were used in the monodisperse version described by Eqs. [1] and [2] and for the fitting procedure smeared by a Gaussian of 6% standard deviation, which should be a good approximation of the experimental resolution. We also did fits using a polydisperse version for the lamellar thickness (where the thickness varied with a Gaussian function around its mean value). Of course, the introduction of this additional fit parameter improves the quality of the fits but there were no substantial features in the experimental data related to the polydispersity parameter. Therefore we think that this additional parameter may be doubtful in its meaning and omitted it in the analysis given in this work.

For all cases the Gaussian profile yields the superior fit (as judged from the residuals) and therefore appears to be the better model for the lamellar film. As an example, both fits are compared in Fig. 3b, where we show the data represented as I^*q^2 vs q and in addition the corresponding residuals. Especially from the residuals it is clear that a much superior fit for the Gaussian model is observed in particular in the range $q = 0.15$–0.22 Å^{-1} (these q-values correspond to real space dimensions of 28–42 Å; i.e., this is the range of the bilayer thickness) but also for larger and smaller q-values. This is not surprising since due to the penetration of the oxyethylene groups into the water one may expect the real profile of the scattering length density to be diffuse, at least for the part of the head groups (22). The results of the data analysis are summarized in Table 1.

The obtained thickness is always about 20% smaller for the diffuse layer model, which appears to be the more realistic model. However, the trends are the same for both models (and it should be noted that the thickness D calculated for the Gaussian model corresponds to an effective thickness that would be obtained for a corresponding rectangular scattering length density profile with a scattering length density equal to the maximum value of the Gaussian profile). Within L_α^+- and $L_{\alpha l}$-phase the thickness decreases somewhat with increasing alcohol content. Upon entering the $L_{\alpha h}$-phase the value becomes significantly smaller, but then increases again upon further increase in the alcohol concentration. The thickness is always smaller than 30 Å and therefore in all the cases significantly lower than the sum of two $C_{12}E_4$ molecules (the stretched alkyl chains would yield 30.8 Å and with the EO chains one would come up with a

TABLE 1

Thickness of the Bilayers as Obtained from Fitting the SANS Data for Samples of $[C_{12}E_4] = 50$ mM and Various Concentrations of Added Benzyl Alcohol, and the Mean Deviation per Data Point for the Different Fits

		Gaussian			Rectangular	
[Alcohol]/mM	Phase	t/Å	D/Å	dev%	D/Å	dev%
16	L_α^+	9.41	23.59	2.07	29.30	4.17
37	L_α^+	9.32	23.36	2.01	28.89	4.22
59	$L_{\alpha l}$	9.05	22.68	2.06	28.36	3.45
80	$L_{\alpha h}$	8.20	20.55	2.89	26.34	2.87
101	$L_{\alpha h}$	8.69	21.78	3.02	27.57	4.74

thickness of 54 Å (1b), thus evidencing that substantial interdigitation of the two monolayers has to take place.

Taking into account the width of the film D and the total amphiphilic volume fraction ϕ_l one can estimate the distance between the different bilayers d as $D = \phi_l d$ (23). For the sample of composition $[C_{12}E_4]$/[alcohol] = 50/16 mM, belonging to the L_α^+ lamellar subregion, one obtains $d = 1200$ Å. The number of shells of the vesicles can be obtained by dividing their radius by the distance d between the bilayers, as known from the FF-TEM pictures (Fig. 2, diameter ≈100–200 nm). For this sample, we have observed a structure of unilamellar vesicles, in agreement with other authors (24).

When the same estimate is made for a sample of the $L_{\alpha l}$ lamellar subregion, with an amount of 150 mM $C_{12}E_4$, we can calculate to have ≈13 shells, in agreement with the picture of multilamellar vesicles. This result should be a good estimate for the same phase for the composition $[C_{12}E_4] = 50$ mM.

III.3. SANS Study of the Quaternary System $C_{12}E_4$/CPyCl/Benzyl Alcohol/D_2O

For a more detailed investigation regarding the structural changes that occur upon introduction of the cationic surfactant cetylpyridinium chloride (CPyCl) into the formerly studied ternary system further SANS measurements were performed. These were done along two lines in the phase diagram (see Fig. 1):

—In the first series the amount of CPyCl was kept constant at 0.2 mM and the amount of benzyl alcohol was varied.

—In the second series the amount of benzyl alcohol was kept constant at 41 mM and the amount of CPyCl was varied.

III.3.1. The system containing 50 mM $C_{12}E_4$/0.2 mM CPyCl. In this series the amount of benzyl alcohol was varied from 0 to 175 mM; i.e., all the different L_α-phases as well as the L_3-phase are covered. The obtained scattering curves (Fig. 4a) look very similar in general for all the different bilayer phases. In all cases a monotonics decrease of the scattering intensity with increasing q is observed. Evidently the introduced charge density of the bilayers is not yet sufficient to introduce a correlation peak between the bilayers (that should be covered by the given q-range).

A more interesting detail is the change of the scattering intensity with changing content of benzyl alcohol. A careful inspection of Fig. 4a reveals that the scattering intensity is almost identical for all three samples within the L_α^+-phase. It is lower in the $L_{\alpha l}$-phase, lowest in the $L_{\alpha h}$-phase, and then increases again for the L_3-phase. For the last sample that is again located within the $L_{\alpha l}$-phase a value similar to the ones for the other samples within the $L_{\alpha l}$-phase is found.

This effect is shown more clearly in Fig. 4b where the intensity at $q = 0.01$ Å^{-1} is given as a function of the amount of added benzyl alcohol. Constant values within the $L_{\alpha l}^+$-phase are followed by intensities for the $L_{\alpha l}$-phase that decrease with increasing concentration of benzyl alcohol. The low value observed in the $L_{\alpha h}$-phase is good in line with an extrapolation from the $L_{\alpha l}$-phase. This could be an indication that actually the $L_{\alpha l}$-phase is in reality a vesicle phase that—with increasing content of benzyl alcohol—contains increasing numbers of planar lamellae. In the $L_{\alpha h}$-phase, then, only planar bilayers are present, and this would be in agreement with the fact that the phase boundary drawn in Fig. 4b is mainly determined on the basis of rheological results. However, as long as there is still a substantial number of bilayers present in the form of vesicles they will dominate the rheological behavior and only when they have more or less completely vanished will a low viscous $L_{\alpha h}$-phase be observed.

Upon crossing into the L_3-phase the intensity jumps up again by almost a factor of 5 and for the $L_{\alpha l}$-phase at high benzyl alcohol concentration a value similar to the ones at low benzyl alcohol concentration is observed.

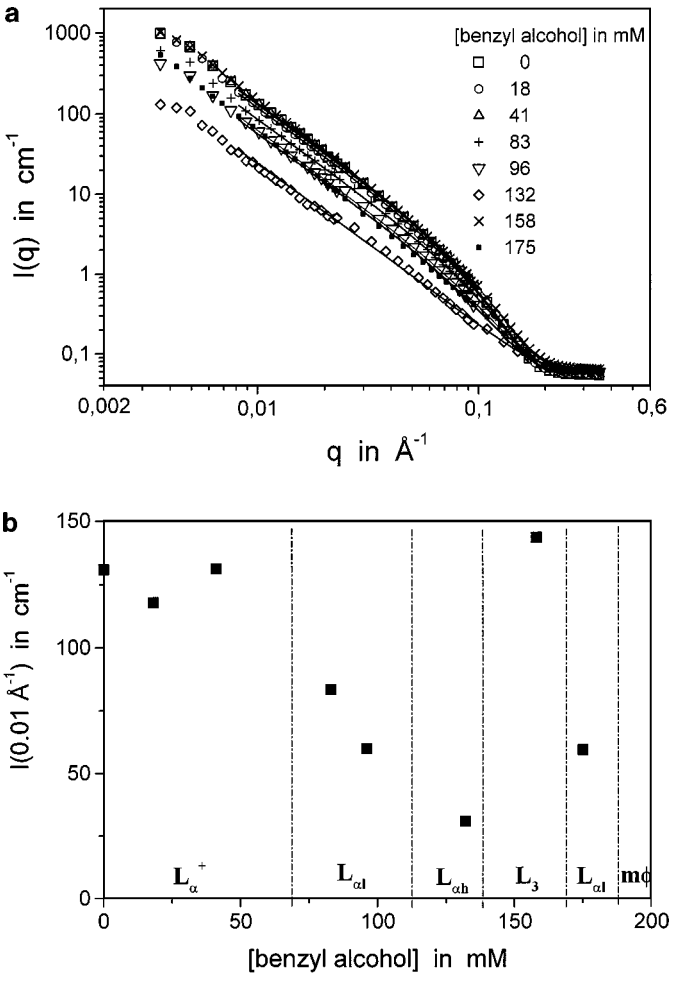

FIG. 4. (a) SANS intensity as a function of the scattering vector q for the system $[C_{12}E_4] = 50$ mM; [CPyCl] = 0.2 mM for various concentrations of added benzyl alcohol (given in the inset). (Fit curves according to the Gaussian distribution of the scattering length density are given as solid lines). (b) SANS intensity at $q = 0.01$ Å^{-1} as a function of the added amount of benzyl alcohol for systems containing 50 mM $C_{12}E_4$ and 0.2 mM CPyCl. The various phases are indicated.

An analysis of the SANS curves shows that they are best described by locally flat 2-dimensional lamellae; i.e., in all cases bilayer systems should be present. In order to obtain quantitative values for the bilayer thickness D we fitted the experimental data (for $q > 0.008$ Å^{-1}) with Eqs. [1] and [2], but in all cases we found again that the fit was significantly better for the model of a diffuse bilayer (Eq. [2]). The obtained values are summarized in Table 2 and they show a trend similar to that of the scattering intensities. This means that D first decreases continuously from about 25 Å for the system without benzyl alcohol to a minimum of less than 19 Å that is reached for the $L_{\alpha h}$-phase. Then D increases again for the sample within the L_3-phase and decreases again for the sample within the $L_{\alpha l}$-phase.

The trend of decreasing thickness with increasing alcohol content is to be expected, since more and more of the bilayer will be made up from the shorter chain alcohol. However, much more interesting are the irregularities at high benzyl alcohol concentration where upon entering the L_3-phase and then the $L_{\alpha l}$-phase again toward higher alcohol concentration the thickness D increases again although the relative content of the alcohol in the bilayer increases. It is also interesting to note that the thickness of the bilayer is similar for the L_α^+-phase and for the L_3-phase.

Assuming a locally flat bilayer one can simply calculate from these thickness values D the head-group area a_h per surfactant molecule (here we have used molecular volumes of 630.4 Å^3 for $C_{12}E_4$, 172.0 Å^3 for benzyl alcohol, and 546.7 Å^3 for CPy—as obtained from the densities of the pure compounds and an estimated density of 0.925 g/ml for the CPy part of CPyCl). These values are also included in Table 2. By this method for the system without benzyl alcohol (50 mM $C_{12}E_4$ and 0.2 mM CPyCl) a value of 50.5 Å^2 has been obtained that compares well with values for the pure $C_{12}E_4$ system of 46 Å^2 (obtained from surface tension measurements at the air–water interface (25)) and 53.8 Å^2 (obtained from SANS experiments on microemulsions with octane at 11°C (26)).

With increasing amount of benzyl alcohol the head group area per surfactant molecule ($C_{12}E_4$ and CPyCl) increases, which means effectively that the benzyl alcohol requires some space

TABLE 2

Volume Fraction of Amphiphilic Material ϕ_l, Phase Type, Fitted Thickness $D = ((2\pi)^{0.5} \times t)$, and Calculated Head Group Area a_h per Surface Molecule for Samples Containing 50 mM $C_{12}E_4$, 0.2 mM CPyCl, and Various Amounts of Benzyl Alcohol (in D_2O)

c(BzOH)	ϕ_l	Phase	ρ in 10^9 cm^{-2}	D in Å	a_h in Å^2
0	0.01905	L_α^+	0.77	25.07	50.5
18	0.02091	L_α^+	1.86	24.73	56.2
41	0.02329	L_α^+	3.00	24.57	63.0
83	0.02765	$L_{\alpha l}$	4.58	23.72	77.4
96	0.02899	$L_{\alpha l}$	4.97	22.39	86.0
132	0.03272	$L_{\alpha h}$	5.89	18.87	115.2
158	0.03541	L_3	6.43	23.91	98.4
175	0.03717	$L_{\alpha l}$	6.75	20.37	121.2

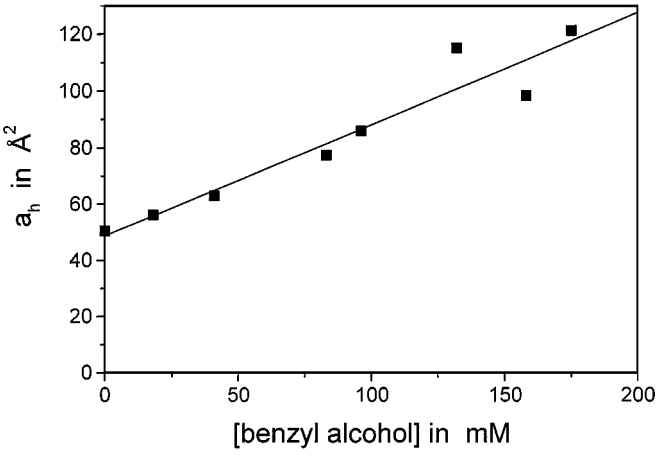

FIG. 5. The head group area a_h per surfactant molecule ($C_{12}E_4$ + CPy) as a function of the amount of added benzyl alcohol.

at the amphiphilic interface. This increases goes linearly with the concentration of benzyl alcohol (Fig. 5). From the slope in Fig. 5 one can conclude that one molecule of benzyl alcohol requires about 19–20 Å^2 as a head group area, a value that is fairly large when compared to those for other cosurfactants (23d) and probably due to the fact that the aromatic ring is fairly bulky.

III.3.2. The system containing 50 mM $C_{12}E_4$/41 mM benzyl alcohol. Here systems were investigated that contained a constant amount of benzyl alcohol and from 0 to 3 mM of added CPyCl. Along this line in the phase diagram the obtained SANS curves (Fig. 6a) change considerably. Again for all cases where bilayers are present the Gaussian model for the scattering length density yields superior results. This is demonstrated in Fig. 6b, which shows as an example residuals for low (0.3 mM) and high (1.2 mM) content of CPyCl. Again in the range $q = 0.13$–0.22 Å^{-1} the Gaussian model is a significantly better description of the experimental data.

At low content of the cationic CPyCl scattering curves similar to those preceding are observed that are typical for systems with locally flat bilayers. However, with increasing content of cationic surfactant, i.e., increasing charge density of the bilayers, a peak becomes visible at ≈ 0.005 Å^{-1}. This peak is the correlation peak of the lamellar phase. The corresponding spacing of 1200 Å is in good agreement with the results of electronmicroscopy in the ternary system and for the given volume fraction of 0.0233 would correspond to a bilayer thickness D of 28 Å for stacked bilayers and this agrees well with the thickness values derived before (Table 2). Fits with Eq. [1] yield a lamellar thickness of about 24 Å that does not change significantly with increasing content of CPyCl (Table 3).

Samples measured within the 2-phase region (before macroscopic demixing has set in) already show a pronounced scattering peak. Such a correlation peak is also observed for still higher CPyCl content for samples in the L_1-phase and the peak moves to higher q-values with increasing content of the cationic CPyCl. This shows that the mean spacing between the aggregates becomes smaller with increasing charge density. Evidently

TABLE 3

Volume Fraction of Amphiphilic Material ϕ_l, Phase Type, Fitted Lamellar Thickness $D = ((2\pi)^{0.5} \times t)$ (Fitted for $q > 0.01$ Å^{-1}), and Rod Radius R (Fitted for $q > 0.055$ Å^{-1}) for Samples Containing 50 mM $C_{12}E_4$, 41 mM Benzyl Alcohol, and Various Amounts of Added CPyCl (in D_2O)

[CPyCl]/mM	ϕ_l	Phase	D in Å	R in Å
0	0.02323	L_α^+	24.0	—
0.2	0.02329	L_α^+	24.2	—
0.3	0.02333	L_α^+	24.3	—
0.4	0.02336	L_α^+	24.3	—
0.75	0.02348	L_α^+	24.0	—
1.05	0.02357	L_α^+	23.5	—
1.2	0.02362	2Φ	22.0	—
2.0	0.02378	2Φ	—	20.9
2.4	0.02402	L_1	—	19.8
3.0	0.02422	L_1	—	18.9

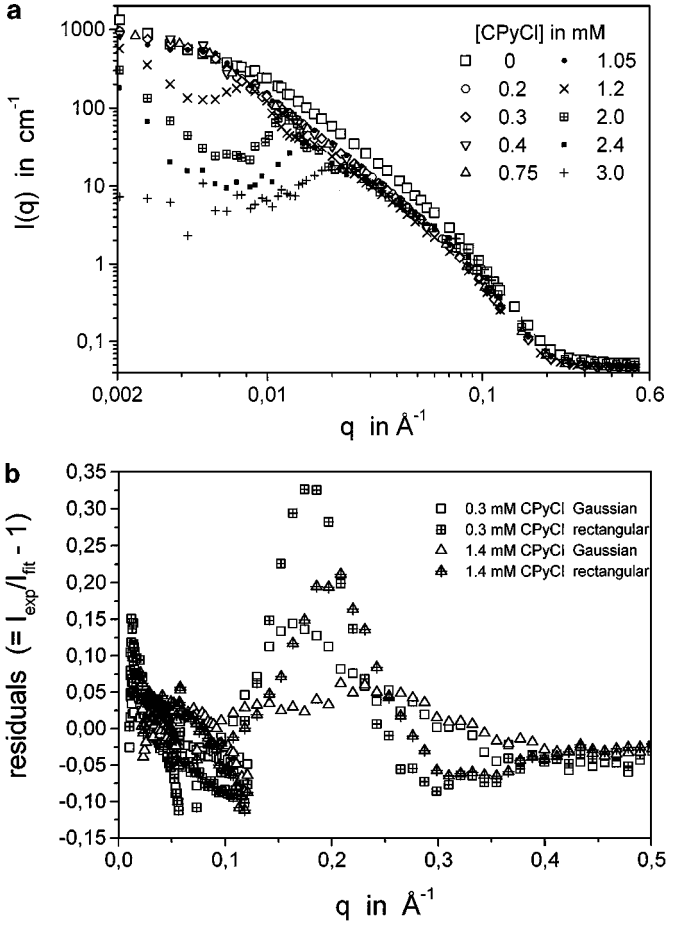

FIG. 6. (a) SANS intensity as a function of the scattering vector q for the system $[C_{12}E_4] = 50$ mM; [benzyl alcohol] = 41 mM for various concentrations of added CPyCl (given in the inset). (b) Residuals (defined by $I_{exp}/I_{fit} - 1$) for the Gaussian and the rectangular model for the distribution of scattering length density as a function of q for samples of composition 50 mM $C_{12}E_4$/41 mM benzyl alcohol and 0.3 or 1.2 mM CPyCl, respectively.

size and shape of the aggregates present change markedly with rising CPyCl concentration.

Rheological investigations of the L_1-phase (11, 19) indicate the presence of rodlike micelles below 5 mM of CPyCl. This is in good agreement with the SANS data. For instance, the peak position at $q_m = 0.022$ Å^{-1} for the 3-mM CPyCl sample would correspond to the interaction peak of long rodlike micelles in a hexagonal ordering with a radius of 26.9 Å, a value that appears reasonable for the given length of the alkyl chains. (It should be noted that this is an upper estimate for the radius since a less dense packing—as it is likely to be present in the system—will lead to somewhat smaller values for the radius, given by

$$R = \frac{1}{q_m}\sqrt{\frac{8 \cdot \pi}{\sqrt{3}}\phi_l}. \qquad [3]$$

Within the L_1-phase the higher q-range of the scattering curves could be fitted well with models of prolate ellipsoids or cylinders. Values for the cylinder radius R obtained with the conventional formula for the form factor of cylinders (27) are given in Table 3 and one finds radii of 19–21 Å which correspond well to the length of the stretched alkyl chains of the surfactant.

In the intermediate range (i.e., within the two-phases region (2ϕ) and also in the L_1 phase in the vicinity of the 2ϕ-region) the peak position and also the scattering behavior at large q-values is not readily explainable just by the presence of rodlike micelles. Here it appears that a mixture of rodlike micelles and vesicles is still present.

IV. CONCLUSIONS

In this investigation the influence of the addition both of a short chain alcohol as a cosurfactant and of a cationic surfactant to an originally nonionic surfactant system has been studied with respect to the aggregate structures present. At the surfactant concentration studied (50 mM) the binary nonionic surfactant forms a vesicle phase. Addition of the alcohol leads to a phase progression of various different bilayer phases ($L_{\alpha l}^+$, $L_{\alpha l}$, and $L_{\alpha h}$). The successive addition of the cationic CPyCl stabilizes vesicle formation relative to the formation of planar bilayers. Therefore the $L_{\alpha l}$-phase extends at the expense of the $L_{\alpha h}$-phase and one even observes the interesting situation that now the addition of further alcohol to an L_3-phase yields a vesicle phase again.

With respect to the thickness of the bilayers one observes first the normal trend that it decreases continuously with increasing alcohol content. But then it decreases rather abruptly for the $L_{\alpha h}$-phase, jumps up for the L_3-phase, and then decreases again at still higher alcohol content for the $L_{\alpha l}$-phase. This is very uncommon behavior as one may expect continuous change with continuous change of the content of benzyl alcohol in the bilayer. One possible explanation for this strange behavior would be that the solubilization site of the benzyl alcohol changes significantly

from one bilayer phase to the other. In the planar lamellar case it would primarily be located at the amphiphilic interface, whereas it would to a much larger degree be solubilized in the bilayer core for the L_3-phase.

The stabilization of the vesicle phase due to the addition of the cationic surfactant is limited to relatively small amounts of cationic surfactant. Once its concentration becomes too large it destabilizes the formation of bilayers altogether (as the pure cationic surfactant would form rodlike micelles) and it triggers a transition to rodlike micelles. At about 5 mol% of cationic surfactant an L_1-phase is formed. In the intermediate range a mixture of bilayer and rodlike structures is formed.

ACKNOWLEDGMENTS

We thank the Laboratoire Léon Brillouin (Saclay) and the Risø National Laboratory for financial help through the large installation program of the European Community. In addition we acknowledge help with the SANS experiments from J. Oberdisse, A. Maldonado, W. Ulbricht, and J. Escalante. Furthermore we are grateful to K. Horbaschek and M. Bergmeier for the preparation of the electron micrographs. G. Montalvo also thanks the Ministerio de Educación y Ciencia for financial support.

REFERENCES

1. (a) Fendler, J. H., and Fendler, E. J., "Catalysis in Micellar and Macromolecular Systems." Academic Press, New York, 1975; (b) Tanford, C., "The Hydrophobic Effect: Formation of Micelles and Biological Membranes," 2nd ed., Wiley, New York, 1980.
2. (a) Mitchell, D. J., Tiddy, G. J. T., Waring, L., Bostock, M. P., Mc Donald, M. P., *J. Chem. Soc. Faraday Trans*. **79,** 975 (1983); (b) Hofland, H. E. J., Bouwstra, J. A., Gooris, G. S., Spies, F., Talsma, H., and Junginger, H. E., *J. Colloid Interface Sci*. **161,** 366 (1993); (c) Strey, R., Jahn, W., Porte, G., and Bassereau, P., *Langmuir* **6,** 1635 (1990).
3. Porte, G., Marignan, J., Bassereau, P., and May, R., *J. Phys. France* **49,** 511 (1988).
4. Jonströmer, M., and Strey, R., *J. Phys. Chem.* **96,** 5993 (1992).
5. Valiente, M., *Colloids Surf. A Physicochem. Eng. Aspects* **105,** 265 (1995).
6. Hoffmann, H., *Ber. Bunsen-Ges. Phys. Chem.* **98,** 1433 (1994).
7. Olsson, U., Nakamura, K., Kunieda, H., and Strey, R., *Langmuir* **12,** 3045 (1996).
8. Hoffmann, H., Munkert, U., Thunig, C., and Valiente, M., *J. Colloid Interface Sci*. **163,** 217 (1994).
9. Montalvo, G., Rodenas, E., and Valiente, M., *J. Colloid Interface Sci*. **202,** 232 (1998).
10. Montalvo, G., Valiente, M., and Rodenas, E., *J. Colloid Interface Sci*. **172,** 494 (1995).
11. Montalvo, G., Rodenas, E., and Valiente, M., *J. Colloid Interface Sci*. **227,** 171 (2000).
12. (a) Lekkerkerker, H. N. W., *Physica A* **159,** 319 (1989); (b) Mitchell, D. J., and Ninham, B. W., *Langmuir* **5,** 1121 (1989); (c) Winterhalter, M., and Helfrich, W., *J. Phys. Chem*. **96,** 327 (1992); (d) Fogden, A; and Ninham, B. W., *Adv. Colloid Interface Sci*. **83,** 85 (1999).
13. Helfrich, W., *J. Phys. Condens. Matter* **6,** A79 (1994).
14. Porte, G., *J. Phys. Condens. Matter* **4,** 8649 (1992).
15. Hoffmann, H., Thunig, C., and Valiente, M., *Colloids Surf.* **67,** 223 (1992).
16. Valiente, M., Thunig, C., Munkert, U., Lenz, U., and Hoffmann, H., *J. Colloid and Interface Sci*. **160,** 39 (1993).
17. Schomäcker, R., and Strey, R., *J. Phys. Chem*. **98,** 3908 (1994).
18. Gradzielski, M., *Langmuir* **14,** 6037 (1998).
19. (a) Montalvo, G., doctoral thesis, University of Alcalá, 1999; (b) Valiente, M., Montalvo, G., Bergmeier, M., Horbascheck, K., Rodenas, E., "Colloid e Interfases Estado líquido." Universidad de Almería, 2000.
20. Olsson, U., and Mortensen, K., *J. Phys. II Fr*. **5,** 789 (1995).
21. Strey, R., Winkler, J., and Magid, L., *J. Phys. Chem*. **95,** 7502 (1991).
22. Danino, D., Talmon, Y., and Zana, R., *J. Colloid interface Sci*. **186,** 170 (1997).
23. (a) Marignan, J., Gauthier-Fournier, F., Apple, J., Akoum, F., and Lang, J., *J. Phys. Chem*. **92,** 440 (1988); (b) Strey, R., Schomäcker, R., Roux, D., Nallet, F., and Olsson, U., *J. Chem. Soc. Faraday Trans*. **86,** 2253 (1990); (c) Bassereau, P., Appell, J., and Marignan, J., *J. Phys. II Fr*. **2,** 1257 (1992); (d) Gradzielski, M., Hoffmann, H., and Langevin, D., *J. Phys. Chem*. **99,** 12612 (1995); (e) Gustafsson, J., Orädd, G., Lindblom, G., Olsson, U., and Almgren, M., *Langmuir* **13,** 852 (1997); (f) Hornfeck, U., Gradzielski, M., Mortensen, K., Thunig, C., and Platz, G., *Langmuir* **14,** 2958 (1998).
24. (a) Hervé, P., Roux, D., Bellocq, A. M., Nallet, F., and Gulik-Krzywicki, T., *J. Phys. II Fr*. **3,** 1255 (1993); (b) Schömacker, R., and Strey, R., *J. Phys. Chem*. **98,** 3908 (1994); (c) Strey, R., *Ber. Bunsen-Ges. Phys. Chem*. **100,** 182 (1996); (d) Oberdisse, J., Regev, O., and Porte, G., *J. Phys. Chem. B* **102,** 1102 (1998).
25. Rosen, M. J., Cohen, A. W., Dahanayake, M., and Hua, X. Y., *J. Phys. Chem*. **86,** 541 (1982).
26. Sottmann, T., Strey, R., and Chen, S. H., *J. Chem. Phys*. **106,** 6483 (1997).
27. Guinier, A., and Fournet, G., "Small-Angle Scattering of X-Rays." Wiley, New York, 1955.